Considerations for Ku-Band Scatterometer Calibration Using the Dry-Snow Zone of the Greenland Ice Sheet

Kevin R. Moon and David G. Long, *Fellow, IEEE*

***Abstract*—Postlaunch calibration of satellite-borne scatterometers using backscatter data from natural land targets helps to maintain scatterometer accuracy. Due to its temporal stability, the dry-snow zone of the Greenland ice sheet has been proposed in previous studies as a calibration target. Using QuikSCAT data, this letter examines the backscatter properties of the dry-snow zone that are relevant to Ku-band scatterometer calibration including temporal and spatial variabilities, and azimuth-angle and polarization and incidence-angle dependences. The backscatter is found to seasonally vary throughout the dry-snow zone by 0.4 dB on average. Small interannual variations (less than 1.5 dB over a nine year period) in the backscatter are also present in some regions. Azimuth modulation is generally less than 0.4 dB in magnitude and is not significant in some regions of the dry-snow zone. Melting and refreezing appear to cause the quasi-polarization ratio to temporarily decrease. Spatially consistent and relatively temporally stable regions that are well within the interior of the dry-snow zone are best suited as calibration sites.**

***Index Terms*—Ice sheet, Greenland, QuikSCAT, scatterometer calibration, snow.**

I. Introduction

SATELLITE-borne scatterometers are microwave radars designed to estimate the wind velocity over the earth's oceans [1]. The wind estimates are useful for studying the earth's climate and for forecasting and monitoring weather patterns including hurricanes. Scatterometers have been also used for tracking icebergs [2], mapping the sea ice extent [3], measuring deforestation in the Amazon [4], and monitoring important indicators of the global climate such as the Greenland [5], [6] and Antarctic [7] ice sheets.

Critical for scatterometer applications is precise calibration [8]. Accurate postlaunch calibration can be achieved by using radar backscatter data from natural land targets with isotropic radar response, temporally constant backscatter during the calibration period, and uniform backscatter over a large area [9]. Temporal stability over longer periods of time is required when recalibrating a scatterometer or when cross-calibrating scatterometers with few coincident measurements. Past calibration sites include the Amazon rainforest, the Greenland and Antarctic ice sheets, and the Sahara desert [9]–[12]. Of these regions, the backscatter in the Antarctic ice sheet and the dry-snow zone of the Greenland ice sheet varies the least [13].

Scatterometers provide consistent and frequent observations of the polar regions where they achieve multiple passes per day due to the converging orbits. The high quantity of measurements in these regions gives further weight to choosing polar ice sheets as calibration locations. Since minimal azimuth-angle dependence is desired for scatterometer calibration, the dry-snow zone of the Greenland ice sheet may be better suited for calibration than the Antarctic ice sheet, which may have higher azimuth-angle dependence [14], [15].

To better understand the capability of the Greenland dry-snow zone as a calibration target, this letter examines the spatial and temporal properties of the dry-snow zone backscatter and azimuth dependence at the Ku-band using data from the QuikSCAT scatterometer. First, background information about QuikSCAT and the electromagnetic properties of the Greenland ice sheet is given. Second, the interannual variability of the dry-snow line and the spatial and temporal variabilities of backscatter within the dry-snow zone are considered, followed by an analysis of azimuthal modulation and a brief discussion of polarization and incidence-angle dependences within this region. This letter concludes with a further discussion of the long-term stability of the backscatter in the dry-snow zone and provides recommendations for potential calibration sites.

II. Background

A. QuikSCAT

Scatterometers measure the normalized radar cross section σ^0 or backscatter, which is a function of the radar operating frequency, the incidence and azimuth angles, the pulse polarization, and the scattering properties of the area illuminated by the antenna beam [16]. SeaWinds on QuikSCAT (referred to as QuikSCAT by convention) is a 13.4-GHz scanning pencil beam scatterometer [17] that operated from July 1999 to November 2009. QuikSCAT has two beams, each with a wide range of azimuth angles. The inner beam is horizontally polarized with a fixed incidence angle of 46°, whereas the outer beam is vertically polarized with an incidence angle of 54°. QuikSCAT has two different resolutions termed "eggs" and "slices." For brevity, we consider only the vertically polarized egg resolution σ^0 measurement, which has an approximate resolution of 25 km by 35 km [18]. This letter uses QuikSCAT data since its stability and long-time series data set make it useful for studying long-term trends in the dry-snow zone Ku-band backscatter properties.

Manuscript received July 30, 2012; revised December 13, 2012; accepted January 14, 2013. Date of publication February 26, 2013; date of current version October 10, 2013.

The authors are with the Department of Electrical and Computer Engineering, Brigham Young University, Provo, UT 84602 USA (e-mail: rmoon@mers.byu.edu; long@ee.byu.edu).

Color versions of one or more of the figures in this paper are available online at http://ieeexplore.ieee.org.

Digital Object Identifier 10.1109/LGRS.2013.2241012

To aid in analysis, we use images from the Scatterometer Climate Record Pathfinder (www.scp.byu.edu) [19]. For QuikSCAT, daily images of Greenland using either morning passes, evening passes, or all passes are available [20]. All-pass enhanced resolution scatterometer image reconstruction (SIR) daily egg images from QuikSCAT processed to have a pixel resolution of 4.45 km are used to study the temporal and spatial properties of σ^0 in the dry-snow zone. Morning and evening images are used to study diurnal variations, while the raw L1B data are used to estimate azimuth modulation. The h-pol and v-pol images are used to study incidence-angle and polarization dependence. For convenience, only years with complete data records are considered (2000–2008).

B. Electromagnetic Properties of Ice and Snow

Ku-band scatterometer measurements are sensitive to the scattering properties of ice and snow. In snow and ice, the presence of liquid water alters σ^0. As liquid-water content increases due to melt, σ^0 is greatly attenuated resulting in decreases in the signal. Refreezing causes σ^0 to increase [5].

The sensitivity of σ^0 to liquid water has been exploited by satellite-borne scatterometers to map melting trends and properties of the Greenland ice sheet. The melt history and other key features have been used to map the location of the facies or zones on Greenland [3], [5], [21]–[23].

The largest ice facie is the dry-snow zone, which is located in the high elevation interior and defined by negligible annual melt [24]. Given that liquid-water content dramatically affects the temporal stability of σ^0 during the melt season in the other ice facies, they are not recommended as calibration targets. In contrast, the dry-snow zone is characterized by relative temporal stability and is thus identified as the calibration target in this letter.

The backscatter from the dry-snow zone does exhibit some spatial and temporal variabilities. Additionally, the location of the boundary of the dry-snow zone may vary from year to year, and σ^0 in the dry-snow zone can be affected by azimuth modulation. These variations can affect the accuracy of the radar calibration and are examined in the succeeding sections.

III. Interannual Variability of the Location of the Dry-Snow Zone Boundary

The dry-snow zone can be mapped by using a melt detection algorithm and altitude thresholding. The melt detection algorithm used for dry-snow classification in this letter is the Q–α method, which performs well at identifying the melt extent [25]. A pixel is classified as dry snow if melt is not detected throughout the entire year and if the altitude is greater than a threshold chosen with the aid of a histogram. Altitude thresholding is performed to mitigate the misclassification of pixels within the ablation zone. Annual results are presented in Fig. 1.

The maps in Fig. 1 demonstrate that there is significant spatio-temporal variability in the dry-snow zone. In particular, the 2002 spatial extent of the dry-snow zone is considerably smaller than in other years due to an anomalous melt event [21]. Refreezing after this melt event caused the formation of an extensive ice layer [6], [21], which affected σ^0 in 2002 and in subsequent years (see Sections V and VII). Excluding this

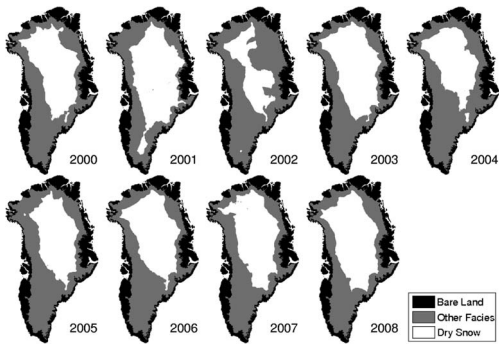

Fig. 1. Maps of the dry-snow zone on the Greenland ice sheet using the Q–α melt detection method and an altitude threshold of 1480 m. (White) Dry snow and the ocean. (Gray) Ice that is not dry snow. (Black) Bare land.

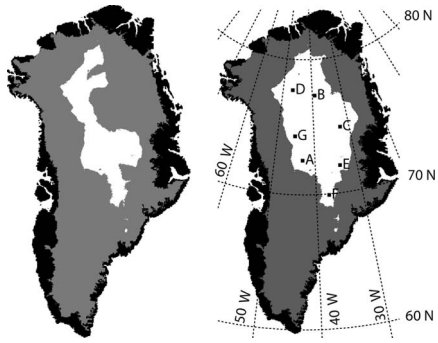

Fig. 2. Region classified as the dry-snow zone common to (left) all years and (right) all years except for 2002. Specific 22-km square analysis points are labeled on the right for detailed study.

year, a general dry-snow region can be determined, although the edges may fluctuate.

For calibration purposes, a region within the interior of the dry-snow zone is particularly recommended if calibration is performed during the summer. This increases the likelihood that the region is actually dry snow, particularly if the current location of the dry-snow zone boundary is unknown. One method for identifying such a region is to use the pixels that are classified as dry snow in all years. Fig. 2 displays a region classified as the dry-snow zone common to the years 2000–2008. This region is fairly small, largely because of the smaller dry-snow zone in 2002. Since 2002 was an anomaly, this year can be excluded to enlarge the area of potential calibration regions for most years. The resulting region is indicated in Fig. 2.

IV. Spatial Variation in σ^0

To investigate the spatial variation in σ^0 (changes in σ^0 with location) in the dry-snow zone, the temporal average of σ^0 over the period of one year (denoted as a) at each pixel is used. Fig. 3 shows values of a for each year from 2000 to 2008. This figure shows that a spatially but coherently varies. The spatial variation is attributed to variations in accumulation rates. In areas within the dry-snow zone with relatively low accumulation, σ^0 is higher than in areas with relatively high accumulation. Low accumulation causes steeper temperature gradients within the upper layers of the firn and exposes the surface snow grains, which may lead to grain size growth [5]. Accumulation also buries subsurface ice structures from past melt and refreeze events resulting in decreased σ^0 over time [6]. Additionally,

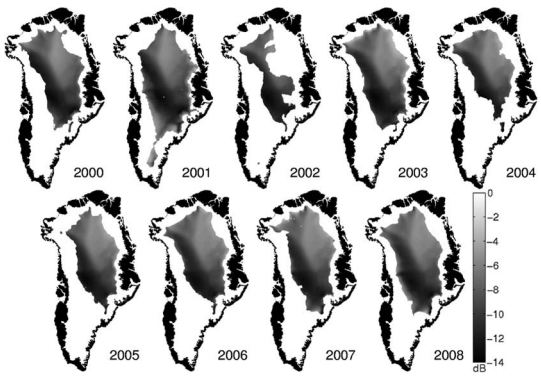

Fig. 3. Temporally averaged backscatter a in decibels over time.

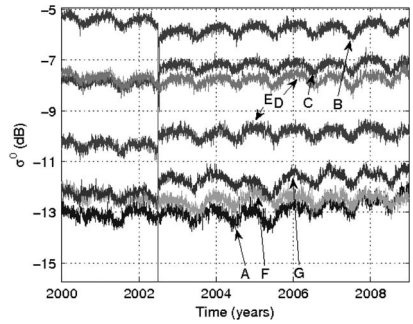

Fig. 4. Spatial mean of σ^0 over time at the seven analysis points (22 km in size) within the dry-snow zone, as shown in Fig. 2. 2002 was an anomalous melt year during which some points fell outside of the dry-snow zone. A strong reset is visible at points C, E, and G after the refreeze season in 2002.

wind scouring of the previous summer surface may contribute to higher backscatter in areas of low accumulation [5] and the formation of sastrugi, which are snow dunes that are formed by wind that lie parallel to the wind direction. Accumulation maps [26] show that the spatial distribution of accumulation rates is consistent with the spatial distribution of a.

The backscatter in the Greenland ice sheet also displays a spatial gradient, which is "the rate of change in the magnitude of the backscatter relative to small changes in geographical location" [14]. The spatial gradient contributes to the spatial variation on a smaller scale. For optimal calibration, the calibration site should include measurements that are as similar to each other as possible. Regions in the dry-snow zone with smaller spatial gradients are recommended for calibration. The magnitude of the spatial gradient limits the size of the calibration site and therefore the amount of measurements used for calibration (assuming a fixed calibration time). Within the dry-snow zone, the spatial gradient is generally less than 0.05 dB/km and is less than 0.01 dB/km in areas with spatially similar values of σ^0. However, if the spatial gradient is stable, then its effects may be corrected within the calibration area. This could allow for larger calibration sites.

For σ^0 uniformity in a region, dry-snow zone calibration sites should be contained within a spatially contiguous region with a spatial variance of σ^0 below the desired value, which depends on the desired accuracy. Previous studies have used 0.5 [9] and 0.15 dB [10] for calibration in the Amazon. We investigate the spatial standard deviation of small regions around the analysis points marked in Fig. 2. The analysis points are chosen to have different values of a and to be contained within the dry-snow zone most of the time. The analysis points all have low spatial standard deviations. The average spatial standard deviation (in decibels) calculated using data from 2000 to 2001 from a 22-km square is 0.14 around point A, 0.10 around points B and C, 0.12 around points E and F, and 0.11 around point G, which is comparable with the value used in [10]. The spatial standard deviation remains relatively constant throughout the QuikSCAT record at points B, D, E, and F. However, by the years 2007 and 2008, the standard deviation is 0.13 at point A, 0.12 at point C, and 0.10 at point G. The increase in the standard deviation at point C coincides with the melt event and subsequent refreezing in 2002, although the standard deviation of other regions is unaffected by this melt and refreeze event in the long run. In general, spatial variability is low when the region is unaffected by melt and refreeze.

V. Temporal Variation in σ^0

Sites with temporally constant σ^0 during the calibration period are desired for scatterometer calibrations. Interannual stability is important for the cross-calibration of scatterometers, that are separated by several years and for recalibration. This section investigates both interannual and intra-annual variations in σ^0 in the dry-snow zone.

A. Interannual Variation in σ^0

Fig. 3 shows that, although the location of the dry-snow line changes, a changes relatively little from year to year. Changes in a are typically gradual over multiple years. The long-term temporal changes in σ^0 can be viewed by plotting the spatially averaged σ^0 over time at the seven analysis points marked in Fig. 2. The backscatter is averaged over a 22-km square at each point and is plotted in Fig. 4. This figure shows that there are small seasonal variations in σ^0 at each analysis point. This seasonal variation is discussed further in Section V-B.

Points A, F, and G are located in the area with the lowest σ^0 (less than -11 dB). At point A, the σ^0 level varies little from year to year from 2000 to 2005. However, from 2005 to 2009, there is an increase of approximately 0.7 dB in the average σ^0 level at this point. Increases in σ^0 around the periphery of the dry-snow zone have typically been associated with a formation of subsurface ice structures associated with a melt event [27]. However, point A is generally far from the boundary of the dry-snow zone, and there is no evidence in the σ^0 record of any melt event in this area from 2000 to 2008. Thus the gradual increase in σ^0 may be due to changes in accumulation patterns in this region. Similar behavior is observed at point G except that the increase in σ^0 is smaller and some melt occurred in 2002. Of all the analysis points, σ^0 is most erratic at point F. Since σ^0 is not particularly stable at points A, F, and G, areas around these locations are not recommended for recalibration or for cross-calibration when the scatterometer records are separated by multiple years.

The average backscatter level around points B, C, D, and E is relatively constant from 2000 to 2002 (ignoring seasonal variations which are discussed later). The anomalous weather pattern in 2002 caused melting to occur around points B, C, and E as evidenced by the decrease in σ^0. After the melt event, the average σ^0 levels are lower in B and higher in C and E than before. The increased σ^0 in C and E is likely due to the ice layer formation previously mentioned. Throughout the remainder of

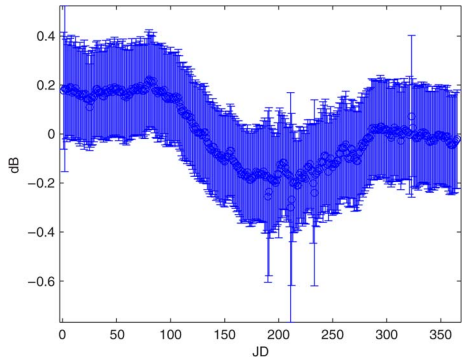

Fig. 5. Spatial average of σ^0 of all pixels in the dry-snow zone in 2000 after removing the pixel means. The error bars denote the standard deviation.

the record, σ^0 at point B slowly increases, whereas σ^0 at points C and E remains roughly constant. The backscatter in point D remains approximately the same throughout the record. This suggests that regions around points C, D, and E may be suitable for recalibration and for cross-calibration as long as no melting has occurred in these regions during the interlude between the two scatterometer records. The region around point B may be acceptable for use as long as melting has not occurred in this region for several years.

B. Intra-Annual Variation in σ^0

Although the temporal variance of σ^0 in the dry-snow zone is low compared with other regions, σ^0 does vary intra-annually. In particular, seasonal variation in σ^0 in the dry-snow zone is evident in Fig. 4. This figure shows that the seasonal variation is characterized by a gradual decrease in σ^0 during the summer months followed by an increase. Seasonal variation in σ^0 is present throughout the entire dry-snow zone. This is clear from spatially averaging σ^0 in the dry-snow zone after subtracting the pixel means.

Fig. 5 shows the spatial average of σ^0 in the dry-snow zone in the year 2000. Although the summer decrease in σ^0 is small (approximately 0.4 dB on average), this seasonal cycle is present throughout the entire dry-snow zone and in all years of QuikSCAT data.

It appears that variations in the average temperature are driving the seasonal variations in σ^0. At temperatures below freezing, the average temperature affects snow density and snow grain growth, which affect σ^0 [7]. Using data from the Greenland Climate Network (GC-Net) [28], the collocated average temperature and σ^0 are found to be negatively correlated. At weather stations within the dry-snow zone that exhibit the seasonal cycle of σ^0, the correlation coefficients of the temporally smoothed temperature and backscatter (using a seven-day moving average) range between -0.6 and -0.9. Further details are provided in [29]. Additional work is required to verify the relationship between the temperature and the seasonal variation in σ^0.

Although the general behavior of the seasonal cycle of σ^0 remains the same, the magnitude and the timing of the seasonal cycle of σ^0 slightly vary from year to year at each pixel. Since temperature and σ^0 are related, *in situ* temperature records may help account for seasonal variation during calibration. If temperature records are not available near the calibration site, then calibration is best performed during the winter or summer months when σ^0 is more temporally stable.

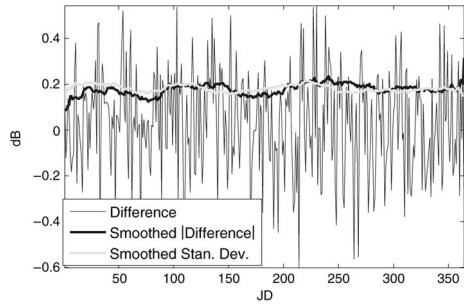

Fig. 6. Difference between morning and evening images, the smoothed magnitude of the difference, and the smoothed spatial standard deviation of the difference in 2008 at point B. Smoothing is performed using a 30-day moving average.

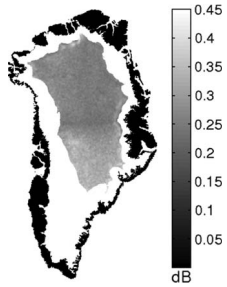

Fig. 7. Average magnitude in decibels of the difference between evening and morning σ^0 images in 2003.

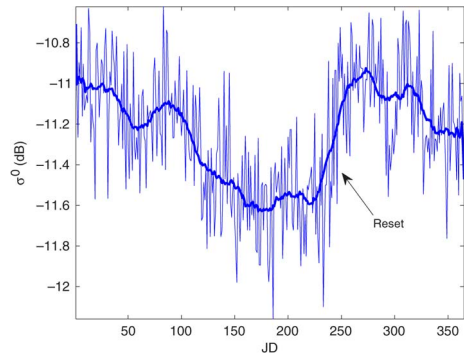

Fig. 8. Backscatter at a single pixel over time in the dry-snow zone in 2003 at 44.7430 °W and 70.6906 °N. This gives an example of seasonal variation and a reset in σ^0 in the dry-snow zone and the noise level. The 30-day moving average is also provided. Short-term temporal variations may be related to temperature.

Since seasonal variations in temperature are related to seasonal variation in σ^0, diurnal variations in temperature may drive diurnal variations in σ^0. QuikSCAT morning and evening images can be used to determine diurnal variations in QuikSCAT σ^0 in the dry-snow zone.

The plot in Fig. 6 shows the difference between morning and evening σ^0 values, the smoothed magnitude of the difference, and the smoothed spatial standard deviation at point B in 2008. This figure shows that the magnitude of the difference between morning and evening images is roughly 0.2 dB on average. However, the difference is noiselike over time with a zero mean. This suggests that daily fluctuations in temperature have little impact on diurnal variation in σ^0. Using the raw L1B data, the normalized standard deviation (K_p) of the QuikSCAT σ^0 values in the dry-snow zone is calculated and found to be

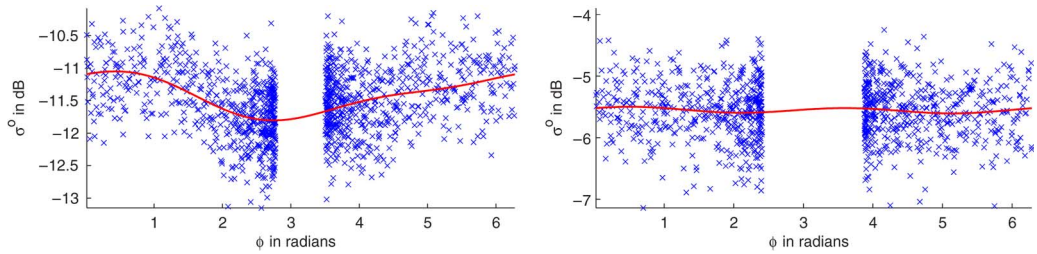

Fig. 9. Scatter plot of σ^0 versus ϕ computed using the model and approach in [14]. (x) Measurements. (Solid line) Estimating second-order azimuth model at points (left) G and (right) B in 2008. The gaps with no data are caused by QuikSCAT's orbit and is related to latitude.

approximately 0.1. This provides an indication of the intrinsic measurement variability and accounts for most of the variability between morning and evening images. Therefore, the observed diurnal variation in σ^0 is mostly attributed to noise.

Fig. 7 shows the temporally averaged magnitude of the difference between morning and evening images of σ^0 in 2003. This serves as an indicator of the spatial distribution of the magnitude of the diurnal variation. This figure shows that the average diurnal variation is spatially coherent with a slightly higher magnitude in the southern region of the dry-snow zone in this year. This suggests that the northern region of the dry-snow zone may be better suited for scatterometer calibration. These results are representative of other years.

Snow accumulation can also affect σ^0 during the year. As previously mentioned, subsurface ice structures (including ice layers) from past melt and refreeze events are buried farther below the surface by accumulation, which results in a decrease in σ^0 throughout the year. This behavior is most common at the edges of the dry-snow zone.

Another temporal behavior sometimes present at the edges of the dry-snow zone is illustrated in Fig. 8. The "reset-like" behavior in σ^0 is characterized by a sudden increase in σ^0 at the end of the summer. Resets typically result in a net increase in σ^0 and are associated with refreeze events in the percolation zone and the wet snow zone. However, small reset-like behavior can be present in the dry-snow zone where there is no apparent melt (see Fig. 8).

VI. Azimuth Modulation

Current scatterometer calibration methods often ignore σ^0 dependence on the azimuth angle ϕ (also called azimuth modulation). Therefore, regions with low azimuth modulation are preferred. Azimuth modulation in the dry-snow zone is likely caused by sastrugi [30]. Sastrugi are snow dunes that are formed by wind that lie parallel to the wind direction. Sastrugi can range in horizontal size from a few to over a hundred meters but are less than 1 m in height [31]. Due to their shape, sastrugi can induce surface scattering that depends on the azimuth angle [15].

Azimuth modulation of σ^0 is small in the Greenland dry-snow zone [14] and larger in Antarctica [15]. In Greenland, azimuth modulation is often modeled using a second-order Fourier series fit as in [14]. For the Ku-band scatterometer NASA Scatterometer (NSCAT), the region in the dry-snow zone with the lowest first- and second-order modulations is limited to the region that runs north and south in the center of the dry-snow zone (see [14, Fig. 6]). Low first-order modulation is slightly more prevalent in the east than in the west.

Azimuth modulation on the Greenland ice sheet may exhibit some variation over time [14]. We look at the azimuth modulation for QuikSCAT at the analysis points identified in Fig. 3.

The model parameters are calculated using data from JD 1 to JD 9. Fig. 9 shows a scatter plot of σ^0 versus ϕ and the estimated model fit at points G and B in 2008. The backscatter clearly depends on ϕ at point G (the first- and second-order magnitudes are approximately 0.3 and 0.1 dB, respectively). However, there is no relationship at point B (0 and 0 dB). Azimuth modulation is also significant at points A (0.3 and 0.1 dB) and E (0.1 and 0.1 dB), significant in the first-order at point F (0.1 and 0 dB), and not significant at points C and D (less than 0.1 and 0.1 dB). These results are consistent with the results obtained from NSCAT [14]. Thus, in terms of azimuth modulation, the areas around points B, C, and D may be better suited as calibration targets.

VII. Discussion

The long- and short-term variabilities of σ^0 in the dry-snow zone, as well as azimuth modulation, have already been discussed. Two other important aspects of backscatter are incidence-angle and polarization dependencies. QuikSCAT has only two different incidence angles, each with different polarizations. Thus, it is difficult to measure variations in the Ku-band incidence-angle and polarization dependencies using QuikSCAT data. However, a general idea of the backscatter dependence on the incidence angle and the polarization can be obtained by comparing QuikSCAT v-pol and h-pol images. Since these images are created using different incidence angles (46° for h-pol and 54° for v-pol), we compute the quasi-polarization ratio defined as v-pol/h-pol. Fig. 10 shows the average quasi-polarization ratio for each year. This figure shows that the ratio in the interior of the dry-snow zone is near unity. Melting and then refreezing in 2002 appear to cause the quasi-polarization ratio to decrease. This can be seen by comparing the values in Fig. 10 in the eastern part of the ice sheet in 2001 and 2003. This is likely caused by ice layer formation, which affects h-pol more than v-pol [6], [21]. As snow accumulation buries the ice layer over several years, the signal from the ice layer is attenuated causing the quasi-polarization ratio to return to near unity.

The recommended sites for recalibration and cross-calibration (B, C, D, and E) are located within the north and northeastern regions of the ice sheet, which is in the precipitation shadow of the topographic barrier [27]. The long-term stability of σ^0 at these sites is likely due to the steady accumulation rates and lack of melting. However, melting and refreezing such as the anomalous event in 2002 can cause a

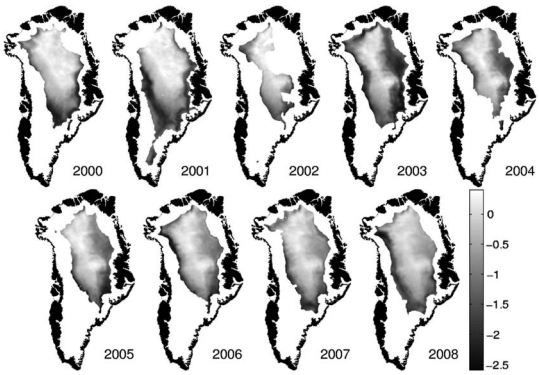

Fig. 10. Average quasi-polarization ratio.

shift in σ^0 (see Fig. 4). Unless the magnitude of the shift can be evaluated, recalibration or cross-calibration in this area may be less accurate in these years or until the accumulation buries the ice layer to sufficient depth. We note that, in 2012, nearly the entire ice sheet experienced some melt [32]. If these extreme melt events become more common, σ^0 in the dry-snow zone of the Greenland ice sheet may lose its long-term stability. Further study of long-term trends in the ice sheet using scatterometers (such as OSCAT) is warranted.

VIII. Conclusion

In summary, the interior of the dry-snow zone where melt is less likely to occur can be used as a calibration site. The regions around points B, C, D, and E demonstrate long-term stability in σ^0 when melt does not occur and may be acceptable for recalibration and cross-calibration. In general, spatially contiguous regions with low spatial variance in σ^0 should be chosen for calibration sites. When melt is not involved, spatial and temporal variations are at a scale of only several tenths of a decibel. However, a $\pm$0.2-dB seasonal variation in σ^0 is present throughout the dry-snow zone and should be accounted for when calibrating scatterometers using the dry-snow zone at different times of year. Azimuth modulation is small throughout the dry-snow zone and is lower in the eastern region.

References

[1] F. Naderi, M. Freilich, and D. Long, "Spaceborne radar measurement of wind velocity over the ocean-an overview of the NSCAT scatterometer system," *Proc. IEEE*, vol. 79, no. 6, pp. 850–866, Jun. 1991.

[2] K. Stuart and D. Long, "Tracking large tabular icebergs using the SeaWinds Ku-band microwave scatterometer," *Deep Sea Res. Part II: Top. Stud. Oceanogr.*, vol. 58, no. 11/12, pp. 1285–1300, Jun. 2011.

[3] D. Long and M. Drinkwater, "Cryosphere applications of NSCAT data," *IEEE Trans. Geosci. Remote Sens.*, vol. 37, no. 3, pp. 1671–1684, May 1999.

[4] D. Long and P. Hardin, "Vegetation studies of the Amazon basin using enhanced resolution Seasat scatterometer data," *IEEE Trans. Geosci. Remote Sens.*, vol. 32, no. 2, pp. 449–460, Mar. 1994.

[5] D. G. Long and M. R. Drinkwater, "Greenland ice-sheet surface properties observed by the Seasat—A scatterometer at enhanced resolution," *J. Glaciol.*, vol. 40, no. 135, pp. 213–230, 1994.

[6] S. Nghiem, K. Steffen, G. Neumann, and R. Huff, "Mapping of ice layer extent and snow accumulation in the percolation zone of the Greenland ice sheet," *J. Geophys. Res.*, vol. 110, no. F2, p. F02017, Jun. 2005.

[7] W. Dierking, S. Linow, and W. Rack, "Toward a robust retrieval of snow accumulation over the Antarctic ice sheet using satellite radar," *J. Geophys. Res.*, vol. 117, no. D9, p. D09110, May 2012.

[8] W. Tsai, J. Graf, C. Winn, J. Huddleston, S. Dunbar, M. Freilich, F. Wentz, D. Long, and W. Jones, "Post-launch sensor verification and calibration of the NASA scatterometer," *IEEE Trans. Geosci. Remote Sens.*, vol. 37, no. 3, pp. 1517–1542, May 1999.

[9] J. Zec, W. Jones, and D. Long, "NSCAT normalized radar backscattering coefficient biases using homogeneous land targets," *J. Geophys. Res.*, vol. 104, no. C5, pp. 11 557–11 568, May 1999.

[10] D. Long and G. Skouson, "Calibration of spaceborne scatterometers using tropical rain forests," *IEEE Trans. Geosci. Remote Sens.*, vol. 34, no. 2, pp. 413–424, Mar. 1996.

[11] R. Kennett and F. Li, "Seasat over-land scatterometer data. II. selection of extended area and land-target sites for the calibration of spaceborne scatterometers," *IEEE Trans. Geosci. Remote Sens.*, vol. 27, no. 6, pp. 779–788, Nov. 1989.

[12] L. Kunz and D. Long, "Calibrating SeaWinds and QuikSCAT scatterometers using natural land targets," *IEEE Geosci. Remote Sens. Lett.*, vol. 2, no. 2, pp. 182–186, Apr. 2005.

[13] R. Kumar, S. Bhowmick, K. Babu, R. Nigam, and A. Sarkar, "Relative calibration using natural terrestrial targets: A preparation towards Oceansat-2 scatterometer," *IEEE Trans. Geosci. Remote Sens.*, vol. 49, no. 6, pp. 2268–2273, Jun. 2011.

[14] I. S. Ashcraft and D. G. Long, "Observation and characterization of radar backscatter over Greenland," *IEEE Trans. Geosci. Remote Sens.*, vol. 43, no. 2, pp. 225–237, Feb. 2005.

[15] D. Long and M. Drinkwater, "Azimuth variation in microwave scatterometer and radiometer data over Antarctica," *IEEE Trans. Geosci. Remote Sens.*, vol. 38, no. 4, pp. 1857–1870, Jul. 2000.

[16] F. Ulaby, R. Moore, and A. Fung, *Microwave Remote Sensing: Active and Passive*. Norwood, MA, USA: Artech House, 1986.

[17] M. Spencer, C. Wu, and D. Long, "Improved resolution backscatter measurements with the SeaWinds pencil-beam scatterometer," *IEEE Trans. Geosci. Remote Sens.*, vol. 38, no. 1, pp. 89–104, Jan. 2000.

[18] I. Ashcraft and D. Long, "The spatial response function of SeaWinds backscatter measurements," in *Proc. SPIE*, 2003, vol. 5151, pp. 609–618.

[19] D. Long, M. Drinkwater, B. Holt, S. Saatchi, and C. Bertoia, "Global ice and land climate studies using scatterometer image data," *EOS, Trans. Amer. Geophys. Union*, vol. 82, no. 43, p. 503, Oct. 2001.

[20] D. Long and B. Hicks, *Standard BYU QuikSCAT and SeaWinds Land/Ice Image Products*, 2010.

[21] L. Wang, M. Sharp, B. Rivard, and K. Steffen, "Melt season duration and ice layer formation on the Greenland ice sheet, 2000–2004," *J. Geophys. Res.*, vol. 112, no. F4, p. F04013, Dec. 2007.

[22] I. Bhattacharya, K. Jezek, L. Wang, and H. Liu, "Surface melt area variability of the Greenland ice sheet: 1979–2008," *Geophys. Res. Lett.*, vol. 36, no. 20, p. L20502, Oct. 2009.

[23] M. Fahnestock, R. Bindschadler, R. Kwok, and K. Jezek, "Greenland ice sheet surface properties and ice dynamics from ERS-1 SAR imagery," *Science*, vol. 262, no. 5139, pp. 1530–1534, Dec. 1993.

[24] C. Benson, "Stratigraphic studies in the snow and firn of the Greenland ice sheet," U.S. Army, Cold Reg. Res. and Eng. Lab., Hanover, NH, USA, SIPRE Res. Rep. Tech. Rep. 70, 1962.

[25] I. Ashcraft and D. Long, "Comparison of methods for melt detection over Greenland using active and passive microwave measurements," *Int. J. Remote Sens.*, vol. 27, no. 12, pp. 2469–2488, 2006.

[26] E. Burgess, R. Forster, J. Box, E. Mosley-Thompson, R. Bromwich, R. Bales, and L. Smith, "A spatially calibrated model of annual accumulation rate on the Greenland ice sheet (1958–2007)," *J. Geophys. Res.*, vol. 115, no. F2, p. F02004, Jun. 2010.

[27] M. Drinkwater, D. Long, and A. Bingham, "Greenland snow accumulation estimates from satellite radar scatterometer data," *J. Geophys. Res. D. Atmosp.*, vol. 106, no. D24, pp. 33 935–33 950, Jan. 2001.

[28] K. Steffen, J. E. Box, and W. Abdalati, "Greenland climate network: GC-Net," CRREL 96-27 Special Report on Glaciers, Ice sheets and Volcanoes, trib. to M. Meier, pp. 98–103 1996.

[29] K. Moon, "Investigations of the dry snow zone of the Greenland ice sheet using QuikSCAT," M.S thesis, Brigham Young Univ., Provo, UT, USA, 2012.

[30] I. Ashcraft and D. Long, "Relating microwave backscatter azimuth modulation to surface properties of the Greenland ice sheet," *J. Glaciol.*, vol. 52, no. 177, pp. 257–266, Mar. 2006.

[31] D. Bromwich, T. Parish, and C. Zorman, "The confluence zone of the intense katabatic winds at Terra Nova Bay, Antarctica as derived from airborne sastrugi surveys and mesoscale numerical modeling," *J. Geophys. Res.*, vol. 95, no. D5, pp. 5495–5509, Jan. 1990.

[32] S. Nghiem, D. Hall, T. Mote, M. Tedesco, M. Albert, K. Keegan, C. Shuman, N. DiGirolamo, and G. Neumann, "The extreme melt across the Greenland ice sheet in 2012," *Geophys. Res. Lett.*, vol. 39, no. 20, p. L20502, Oct. 2012.